

# Synthesis, Characterization and Thermal Behavior of HYP207·3H<sub>2</sub>O Electrical Properties of HYP207

Rahma Rahzelli Zrelli (✉ [rahmazrelli@yahoo.fr](mailto:rahmazrelli@yahoo.fr))

Université de Carthage Faculté des Sciences de Bizerte: Universite de Carthage Faculte des Sciences de Bizerte <https://orcid.org/0000-0002-5620-2408>

**Fathia Chehimi-Moumen**

Université de Carthage Faculté des Sciences de Bizerte: Universite de Carthage Faculte des Sciences de Bizerte

**Dalila Ben Hassen-Chehimi**

Université de Carthage Faculté des Sciences de Bizerte: Universite de Carthage Faculte des Sciences de Bizerte

**Malika Trabelsi-Ayadi**

Université de Carthage Faculté des Sciences de Bizerte: Universite de Carthage Faculte des Sciences de Bizerte

---

## Research Article

**Keywords:** diphosphate, X-ray diffraction, infrared spectroscopy, thermal behavior, optical properties, electrical properties

**Posted Date:** March 23rd, 2021

**DOI:** <https://doi.org/10.21203/rs.3.rs-299265/v1>

**License:** © ⓘ This work is licensed under a Creative Commons Attribution 4.0 International License.

[Read Full License](#)

---

# Abstract

The synthesis of the diphosphate  $\text{HYP}_2\text{O}_7 \cdot 3\text{H}_2\text{O}$  was made via soft chemistry route from evaporation of aqueous solution at room temperature. The obtained compound, was characterized by means of X-ray diffraction (XRD) and infrared spectroscopy (IR). The results showed a high purity phase. IR spectrum of this diphosphate revealed usual signals related to  $\text{P}_2\text{O}_7$  diphosphate group and water molecules.

The thermal decomposition of the synthesized product by DTA / TG proceeded through four stages leading to the formation of the  $\text{Y}_2\text{P}_4\text{O}_{13}$  as a final product. On the other hand, its decomposition by CRTA took place in three stages leading to the formation of the anhydrous diphosphate  $\text{HYP}_2\text{O}_7$  as a final product. X-ray powder diffraction and infrared spectroscopy were used to identify these materials. Furthermore the electrical properties of the  $\text{HYP}_2\text{O}_7$  were investigated through impedance complex analysis. Modest conductivity has been observed in this material at relatively medium temperature range. Activation energy of 0.67 and 1.44 eV, was deduced from the corresponding Arrhenius plot.

The optical band gap of the title compound is calculated and found to be 2.71 eV.

# Introduction

Much scientific disciplines are now concerned with phosphor compounds and / or ionic conductors. Several types of host materials for rare earths are studied: oxides, sulphates and phosphates. Their applications are many and varied.

In this context, rare earth phosphates have been the subject of much research in order to investigate their electrical and optical properties. In the lighting field, fluorescent lamps have been manufactured using lanthanum phosphate doped with  $\text{Ce}^{3+}$  and  $\text{Tb}^{3+}$  ions ( $\text{LaPO}_4: \text{Ce}^{3+}, \text{Tb}^{3+}$ ) [1]. The compound  $\text{CsPrP}_4\text{O}_{12}$  was used in scintillators [2]. Glassy phosphates are also used as laser materials such as  $\text{NaPO}_3$ ,  $\text{Al}(\text{PO}_3)_3$  doped with  $\text{Nd}^{3+}$  [3-4] ions,  $\text{Y}(\text{PO}_3)_3$  doped with  $\text{Yb}^{3+}$  ions [5]. They are also used in medicine, as optical tracers or in the treatment of cancer by target molecule [6].

The present work is part of the search for new multifunctional rare earth phosphates with electrical and optical properties of interest for industrial applications.

In this paper, we describe synthesis, characterization spectroscopic properties and thermal decomposition of  $\text{HYP}_2\text{O}_7 \cdot 3\text{H}_2\text{O}$ . The anhydrous product  $\text{HYP}_2\text{O}_7$  was also prepared and investigated by impedance complex analysis.

# Experimental

## *Synthesis*

An aqueous solution (0.125 M) of  $\text{Na}_4\text{P}_2\text{O}_7$  (Merck, 98 %) was first passed through an ion exchange resin in its H state (Amberlite IR 120). The obtained diphosphoric acid ( $\text{H}_4\text{P}_2\text{O}_7$ , 20 mL) was then rapidly added to a mixture of yttrium chloride ( $\text{YCl}_3 \cdot 6 \text{H}_2\text{O}$ , Merck, 99.9 %) aqueous solution (12 mL,  $4 \cdot 10^{-2}$  M) and ammonia ( $\text{NH}_4\text{OH}$ , Scharlau) solution (10 ml,  $6 \cdot 10^{-1}$  M). The mixture was slowly evaporated at room temperature over five days, after which homogenous and colorless prism deposited. They were filtered off and washed with distilled water.

### **X-ray powder diffraction**

Powder X-ray diffraction pattern was recorded, at room temperature, in the  $2\theta$  range of  $10-60^\circ$  by Panalytical X'Pert PRO MPD diffractometer.

### **Spectroscopic technics**

The functional vibrations groups are examined through Fourier Transform Infrared spectral analysis at room temperature in the range  $400-4000 \text{ cm}^{-1}$  using the NICOLET IR 200 FT-IR infrared spectrometer. The optical absorption is studied at room temperature with a Perkin Elmer Lambda 11 UV/Vis spectrophotometer in the range of 200–400 nm.

### **Thermal Analysis**

Thermal analysis by DTA/TG was performed under argon atmosphere, on a finely ground sample of mass 10.26 mg. The sample was heated in a platinum crucible at a rate of  $5^\circ \cdot \text{min}^{-1}$  in the  $[25 - 900^\circ\text{C}]$  temperature range.

The experiments by controlled rate of thermal analysis (CRTA) were carried out with 50 mg samples weighed into a fused silica cell which was placed into a refrigerated furnace constructed in house and operating in the  $-30 - 600^\circ\text{C}$  temperature range. Once the equilibrium temperature was reached, the pressure above the sample was lowered using vacuum pumping system from 1 bar to  $5 \cdot 10^{-3}$  mbar. During the CRTA experiment, where the decomposition led to the production of vapor, the vapor pressure was measured by a Pirani gauge placed in proximity of the sample. The pressure signal produced by the Pirani gauge was sent to the furnace heating controller. The heating of the sample then took place in such a way as to keep constant at a preset value the vapor pressure generated by the sample. The use of a diaphragm, placed between the Pirani gauge and the vacuum system, permitted an increase of the residual pressure (5 mbar) above the sample without changing the rate of vapor elimination.

### **Impedance Spectroscopy**

Electrical conductivity measurements were performed with a Hewlett-Packard 4192 A impedance analyzer.

# Results And Discussion

## *X ray Diffraction*

The X-ray patterns of the obtained crystals are identical to those of the acidic gadolinium diphosphate trihydrate  $\text{HGdP}_2\text{O}_7 \cdot 3\text{H}_2\text{O}$  type II [7-9]. So the prepared compound is identified as  $\text{HYP}_2\text{O}_7 \cdot 3\text{H}_2\text{O}$  isostructural with the last compound.

Its cell parameters were calculated on the basis of its powder diffractogram starting from the cell parameters of  $\text{HGdP}_2\text{O}_7 \cdot 3\text{H}_2\text{O}$ . The indexed diffractogram and the cell parameters obtained are given in **Table 1**.

## *IR Absorption Spectroscopy*

The infrared spectrum of diphosphate  $\text{HYP}_2\text{O}_7 \cdot 3\text{H}_2\text{O}$  is shown in **Fig.1**, this spectrum exhibit broad bands in the region ( $3476-3191 \text{ cm}^{-1}$ ), which correspond to the stretching of water molecules  $\nu(\text{H}_2\text{O})$ . The spectral region  $2900-2000 \text{ cm}^{-1}$  shows bands due to the  $\text{PO}-\text{H}$  vibrations as well as several weak and medium intensity bands due to the presence of multiple hydrogen bonds. The vibrational band at  $1627 \text{ cm}^{-1}$  correspond to the bending of water molecules  $\delta(\text{H}_2\text{O})$ . The asymmetric and symmetric terminal stretching vibrations of the  $\text{PO}_3$  groups occur in the region  $1250-935 \text{ cm}^{-1}$ . The  $\delta(\text{PO}_3)$  mode is observed in three bands located at  $627, 534$  and  $474 \text{ cm}^{-1}$ .

## **Thermal analysis by TG/DTA**

**Fig.2** shows both TG and DTA thermograms of  $\text{HYP}_2\text{O}_7 \cdot 3\text{H}_2\text{O}$  carried out in argon atmosphere from room temperature to  $900^\circ\text{C}$ .

In the TG curve the weight loss can be divided into four areas:  $27-91^\circ\text{C}$ ,  $91-204^\circ\text{C}$ ,  $204-485^\circ\text{C}$ , and  $485-796^\circ\text{C}$ . The TG weight loss in the first stage (6.6 %) would correspond to the removal of two water molecules (%th = 11.32 %). It is related to the endothermic peak at  $79^\circ\text{C}$ . The second one occurs between  $91$  and  $204^\circ\text{C}$  and is accompanied by an endothermic peak at  $112^\circ\text{C}$ . The corresponding water loss 9.9 % is close to the theoretical value calculated for the loss of two crystallization water molecules. The third and the fourth stages would correspond to the departure of 0.5 water molecule per formula unit (%exp = 2.2 %, %th = 2.83). They are accompanied by a large thermal effect.

So, the total weight loss in  $27-796^\circ\text{C}$  temperature range (19.9 %) would correspond to the loss of the three crystallization water molecules and of the half constitution water molecule, which is in agreement with the calculated value 19.81 %.

The product obtained at the end of the thermolysis has a complex IR spectrum (**Fig.3**). It particularly shows a wide band between  $960$  and  $1320 \text{ cm}^{-1}$  and two bands of low intensity between  $800$  and  $750 \text{ cm}^{-1}$ . The analysis of its powder X-ray diffractogram (**Fig.4**) shows that it is a well crystallized product.

So we can say that the thermal effect appearing between 685 and 900°C is an exothermal one peaking at 802°C and corresponding to the crystallisation of the decomposition product. According to the decomposition equation the final product would be of stoichiometry (Y<sub>2</sub>O<sub>3</sub>,2P<sub>2</sub>O<sub>5</sub>):



The comparison of the obtained patterns with those found in the literature showed that they have no correspondence in the database. So the decomposition product may correspond to a new salt of formula Y<sub>2</sub>P<sub>4</sub>O<sub>13</sub>. It should be noted that in a previous work [10] we have studied the thermal decomposition of HGdP<sub>2</sub>O<sub>7</sub> · 2H<sub>2</sub>O · NH<sub>3</sub> and we have reported the formation of a gadolinium tetrphosphate Gd<sub>2</sub>P<sub>4</sub>O<sub>13</sub> identified by X-ray diffraction (00-035-0078 JCPDS file). This salt has been so far reported as equilibrium phase in the gadolinium phosphate system Gd<sub>2</sub>O<sub>3</sub>-P<sub>2</sub>O<sub>5</sub> and shown to be a defined congruent fusion compound [11]. It seems that the gadolinium tetrphosphate and the new obtained one are not isostructural.

To better specify the influence of water vapor on the decomposition stages of ytterium acid diphosphate trihydrate, we undertook this study using thermal analysis at controlled transformation rate (CRTA).

### Thermal behavior by CRTA

The CRTA curves of the synthesized gadolinium diphosphate obtained under a residual vapor pressure of 5 mbar are shown in **Fig.5**. The temperature curve (I) shows the sample temperature variation with time, controlled so as to keep constant the pressure (curve II). The variation in slope of the temperature curve as well as the regulation changes, that appear in the pressure curve, allow the delimitation of three decomposition steps occurring respectively between -30 – 98 °C (A–B), 98 – 330 °C (B–C), 330 – 525 °C (C–D). The length ratio of steps (AB), (BC) and (CD) is 4 / 1 / 1, respectively.

The IR spectrum and the X-ray patterns of the CRTA residue are shown, respectively, in **Figs. 6 and 7**.

The IR spectrum of the obtained product (**Fig.6**) shows the persistence of the characteristic bands of the diphosphate anion and the decrease of the O-H intensity band.

The corresponding X-ray patterns (**Fig.7**) are found to be identical to those given of the anhydrous diphosphate HGdP<sub>2</sub>O<sub>7</sub> [13].

So, we can conclude that the vapor phase existing under the sample during its decomposition is constituted only by water vapor. This permit to affirm that the sample decomposition took place at a constant rate. In this condition, the weight loss at such step is proportional to the time. Thus, the first and the second steps would be related to the removal of two and half water molecules respectively.

The IR spectra of the products isolated at 98 and 330°C (**Fig.9**) show both characteristic bands of the diphosphate group and those of the crystallization water. The corresponding X-ray Patterns (**Fig.8**) show the formation of well crystallized diphosphates. According to the CRTA results, these diphosphates would

be the monohydrate and the hemihydrate respectively. It seems that their structures are similar to those of anhydrous salt considering the similarity between the corresponding RX patterns and those of the anhydrous product.

The comparison of our results with those found for  $\text{HGdP}_2\text{O}_7 \cdot 3\text{H}_2\text{O}$  [12] show that the decomposition scheme of the two salts are different in spite of their isotypy. Indeed, it was found that the first decomposition step in  $\text{HGdP}_2\text{O}_7 \cdot 3\text{H}_2\text{O}$  by CRTA under 5 mbar water vapor correspond to the removal of only one water molecule. This first water molecule leaved the salt without changing its structural arrangement because it was loosely bounded [7]. A dehydrate isostructural with the initial trihydrate salt was then obtained [13]. This difference between the two CRTA results shows that the water molecules of crystallization are bound differently in the two diphosphate crystal lattices, despite being isostructural.

### Optical study

The UV–Vis electronic spectrum of the studied compound,  $\text{HYP}_2\text{O}_7 \cdot 3\text{H}_2\text{O}$  are reported respectively in **Figs. 10.a-b**. **Fig.10.a** illustrating the absorption spectrum show three absorption bands: an intense one observed at 290 nm and two other large ones with maxima located respectively at 470 and 531 nm. Indeed the neutral yttrium has the electronic structure  $1s^2 2s^2 2p^6 3s^2 3p^6 4s^2 3d^{10} 4p^6 5s^2 4d^1$ . Trivalent yttrium has electronic structure  $1s^2 2s^2 2p^6 3s^2 3p^6 4s^2 3d^{10} 4p^6$ . Therefore no f-f or f-d type transition is expected for this compound.

Consequently, the bands observed on the absorption spectrum of this compound show an energy transfer between Y-Y or Y-O.

The band gap between HOMO (the ability to provide electron) and LUMO orbital (the ability to accept electron) was determined using Tauc method [14] (**Fig.10b**). The value determined is 2.71 eV. As well as, it has the character of a semiconductor with a wide band gap suggesting applications in optoelectronics.

### Electrical properties

The electrical properties of  $\text{HYP}_2\text{O}_7$  were investigated through impedance complex analysis.

In **Fig.11** are shown some Nyquist plots of the anhydrous compound  $\text{HYP}_2\text{O}_7$  at different temperatures. Table.2 gathers the values of the ionic conductivity of this sample at different temperatures.

The Arrhenius diagram is illustrated in figure 12. It is formed by two linear curves with a meeting point located at  $T_r = 874$  K. Such a break is generally due to a crystal structure transition. However, an X-ray diffraction study carried out on a sample calcined at a temperature slightly above the breaking point temperature ( $T_r$ ), shows that no transition of crystal structure has taken place. Furthermore, no thermal accident was observed on the differential thermal analysis curve of  $\text{HYP}_2\text{O}_7$  between 773 and 923 K. The activation energy was determined in the two intervals. We give in Table II the average activation energy value for  $T < T_r$  and  $T > T_r$  as well as the conductance value of this anhydrous phosphate.

According to the literature a similar compound has been studied:  $\text{HGdP}_2\text{O}_7$  [10].

We notice that the gadolinium and yttrium diphosphates have very similar activation energy and conductivity values. This result can be justified by the fact that these two diphosphates have the same crystal structure.

## References

- [1] M. K. Heike, A. Riwozki, S. Kornowski, M. Naused, 1521-4095 (1999)
- [2] A. K. Padhi, K. S. Nanjundaswamy, J. B. Goodenough, J. Electrochem. Soc. 144, 1188-1194 (1997)
- [3] J.E. Marion, M.J. Weber Eur. J. Solid State Inorg. Chem. 28, 271-287 (1991)
- [4] J. H. Campbell, T.I. Suratwala, J. Non-Cryst. Solids 263 - 264, 318-341 (2000)
- [5] R. Ternane, M. Ferid, Y. Guyotc, M. Trabelsi-Ayadi, G. Boulon. Jour of Lumines 128, 387–393(2008)
- [6] S. A Cotton, J. M. Harrowfield, Encyclopedia of Inorg and Bioinorg Chem. 1-7 (2012)
- [7] E.G. Afonin, N. I. Pechurova, Russ. J. Inorg. Chem. 35, 7835 (1990)
- [8] F. Chehimi-Moumen, M. Ferid, D. Ben Hassen-Chehimi, M. Trabelsi-Ayadi, Mater. Res. Bull., 36, 365-373 (2001)
- [9] S. Hraiech, F. Chehimi-Moumen, C. Goutaudier, D. Ben Hassen-Chehimi, M. Trabelsi-Ayadi. Solid. State. Sci. 10, 991 (2008)
- [10] R. Zrelli-Annabi, F. Chehimi-Moumen, H. Moutaabbid, O. Kurakevych, Y. Le Godec, D. Ben Hassen-Chehimi, M. Trabelsi-Ayadi, *Phos Sul and Sili and the Rela Elem*, 194 (2017)
- [11] D. Agrawal, J. Hummel, Electrochem. Soc. 127, 1550-1554 (1980)
- [12] F. Chehimi-Moumen, M. Ferid, D. Ben Hassen-Chehimi, M. Trabelsi-Ayadi, Mater. Res. Bull., 36, 2175-2181 (2001)
- [13] F. Chehimi-Moumen, Philip L Llewellyn, F. Rouquerol, M. Trabelsi-Ayadi, Jour of ther Analy and Calor. 82 (2005)
- [14] J. Tauc, Mater Res Bull 3:37–46 (1968)

## Tables

**Table 1:** Indexing the powder diffractogram of  $\text{HYP}_2\text{O}_7 \cdot 3\text{H}_2\text{O}$

a = 6.403 (4); b = 6.877(5); c = 9.776 (6) Å

$\alpha = 98.43 (4)$ ;  $\beta = 99.60 (4)$ ;  $88.01(5)^\circ$

<b>h k l</b>	<b>d<sub>obs</sub> / Å</b>	<b>d<sub>cal</sub> / Å</b>	<b>I / I<sub>0</sub></b>
0 0 1	9,61	9,54	100
0 1 0	6,83	6,80	2
0 $\bar{1}$ 1	5,59	5,55	1
1 0 1	4,94	4,91	2
0 0 2	4,79	4,77	12
$\bar{1}$ $\bar{1}$ 1	4,59	4,59	1
$\bar{1}$ 1 1	4,21	4,20	1
1 0 2	3,54	3,54	7
0 $\bar{2}$ 0	} 3,41	3,40	6
0 2 0			
0 1 2	3,67	3,67	4
1 $\bar{1}$ 2	3,28	3,27	1
0 0 3	3,19	3,18	13
$\bar{2}$ 0 0	3,16		2
0 2 1	3,06	3,07	2
$\bar{1}$ 2 0	2,991	2,981	1
2 1 0	} 2,878	2,875	2
$\bar{1}$ $\bar{2}$ 2		2,825	2,817
0 1 3	2,733	2,735	1
1 0 3	2,679	2,670	2
2 1 1	2,603	2,606	1
1 1 3	2,394	2,393	8
$\bar{1}$ 0 4	2,368	2,362	3
$\bar{1}$ $\bar{1}$ 4	2,343	2,339	1
$\bar{1}$ $\bar{3}$ 1	2,181	2,180	1
$\bar{1}$ 1 4	2,137	2,137	2
$\bar{1}$ 2 3	2,125	2,125	3
$\bar{1}$ $\bar{3}$ 2	2,108	2,109	1
$\bar{1}$ $\bar{2}$ 4	2,082	2,087	1
$\bar{3}$ 1 2	1,925	1,927	2
$\bar{1}$ $\bar{2}$ 5	1,784	1,784	1
2 $\bar{1}$ 4	1,756	1,755	2
3 1 2	1,738	1,737	1

Table 2: Values of ionic conductivity at different temperatures for HYP<sub>2</sub>O<sub>7</sub> ( $\sigma/S = 5,9 \cdot 10^{-2} \text{ cm}^{-1}$ )

Température T(K)	Résistance R( $\Omega$ )	Conductivité $\sigma$ ( $10^{-8}$ S.cm $^{-1}$ )
686	884377	6,75
697	636007	9,39
718	508806	11,74
724	471528	12,67
732	451968	13,21
747	401778	14,869
757	357885	16,69
763	331583	18,017
773	300135	19,90
783	263219	22,69
793	233192	25,62
801	207239	28,827
822	161122	37,08
833	145745	40,99
843	126536	47,24
852	116469	51,29
862	102116	58,50
872	91465	65,32
886	69128	86,42
897	61473	97,18
907	52836	113,07
917	44405	134,54
927	34835	171,51
937	26377	226,49

**Table 3:** Conductivities and average activation energies of HLnP<sub>2</sub>O<sub>7</sub>

Sample	Tt (K)	Activation energy Ea (eV)		$\sigma(10^{-8} \text{ S.cm}^{-1})$
		T<Tr	T>Tr	
HGdP <sub>2</sub> O <sub>7</sub>	839	0.66	1.16	9.91(T = 734K)< $\sigma$ <251.93 (T = 947K)
HYP <sub>2</sub> O <sub>7</sub>	874	0.67	1.44	6.75(T = 734K)< $\sigma$ <226.49 (T = 937K)

## Figures

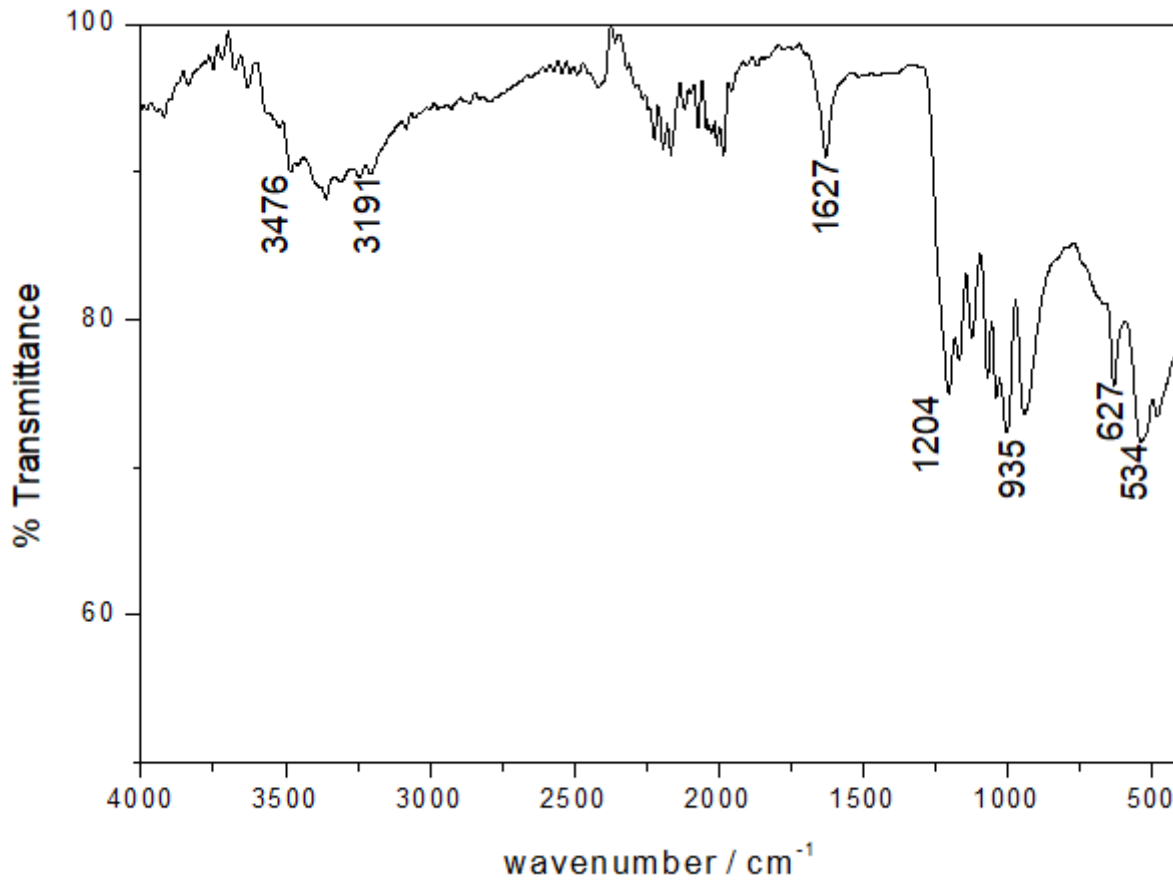


Figure 1

IR spectra of HYP2O7·3H2O

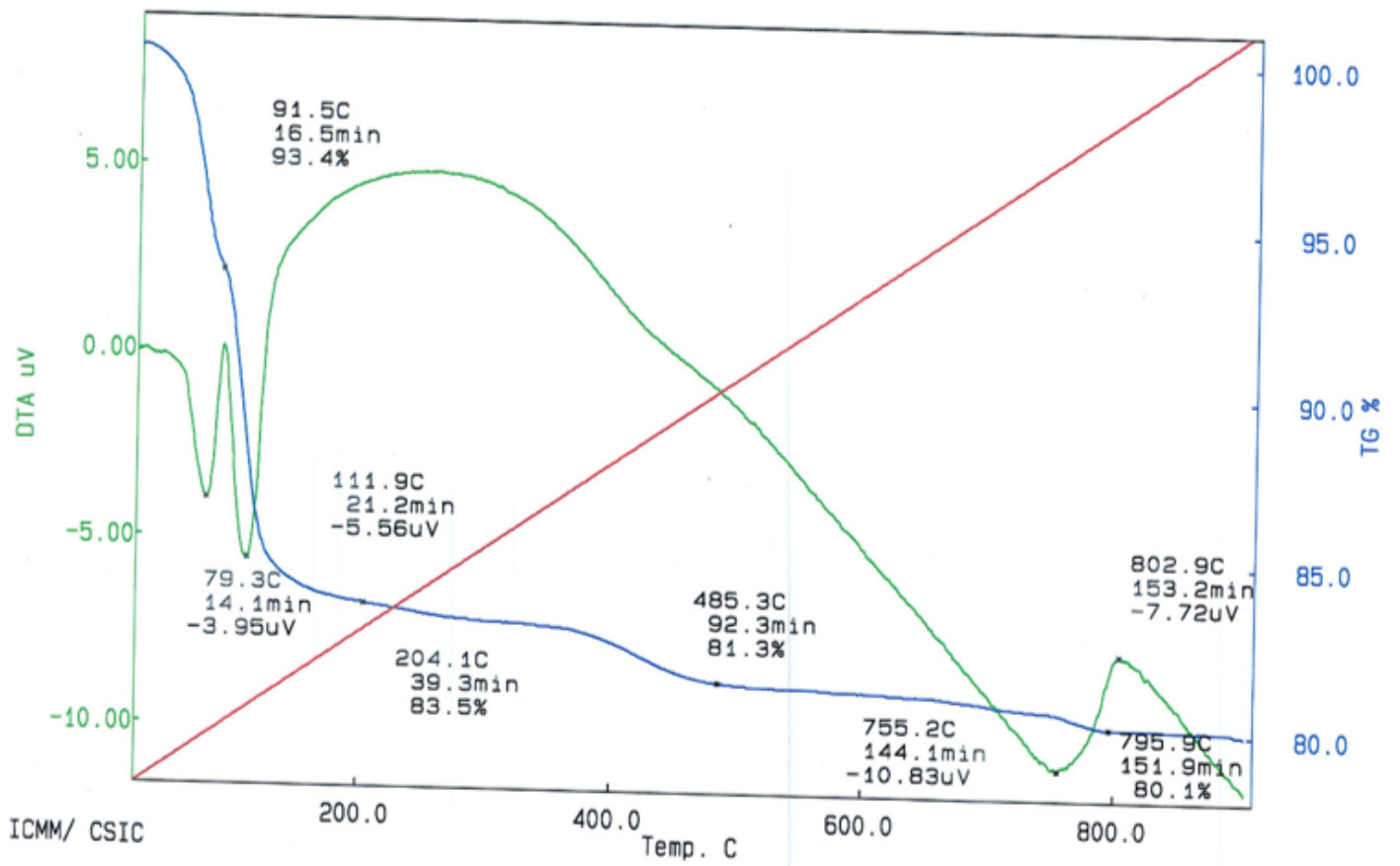
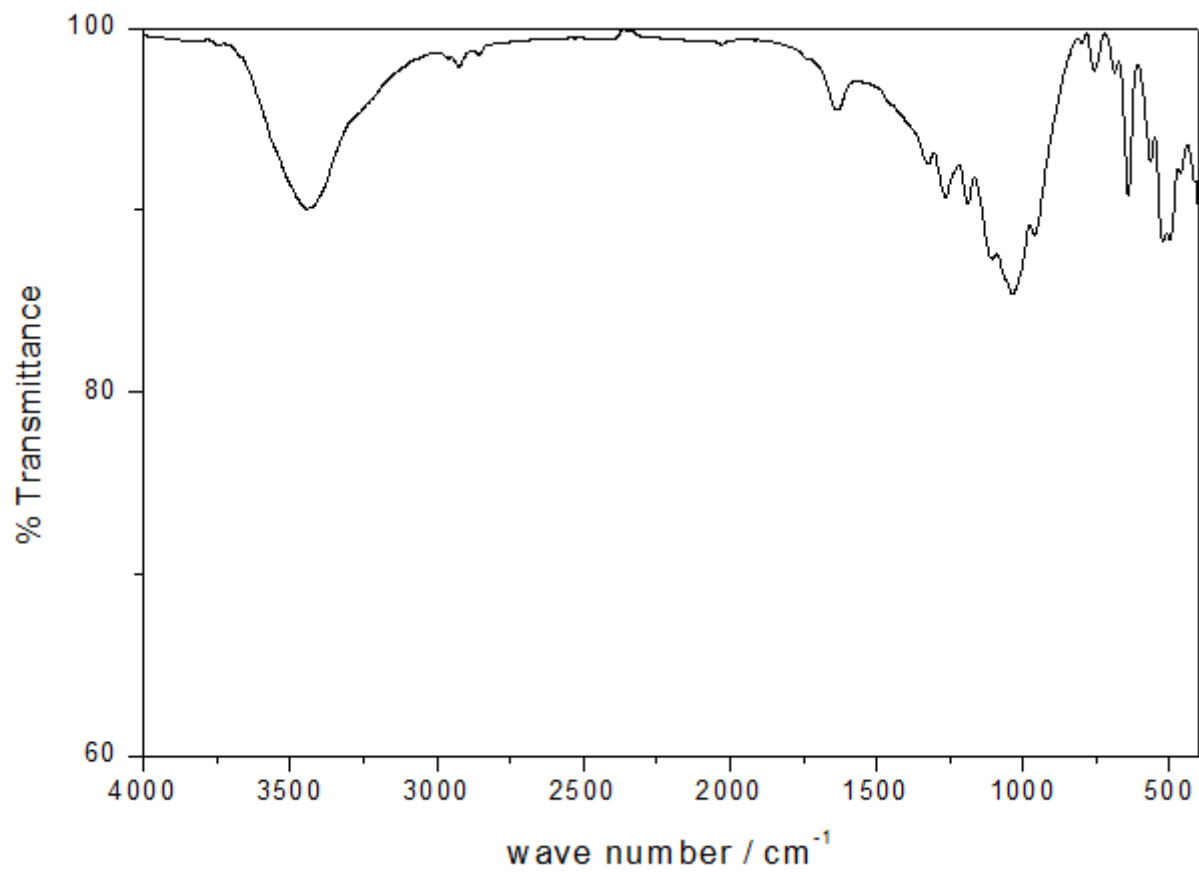


Figure 2

TG and DTA of HYP207·3H<sub>2</sub>O



**Figure 3**

IR spectrum of the thermolysis residue of HYP207·3H<sub>2</sub>O by TG / DTA

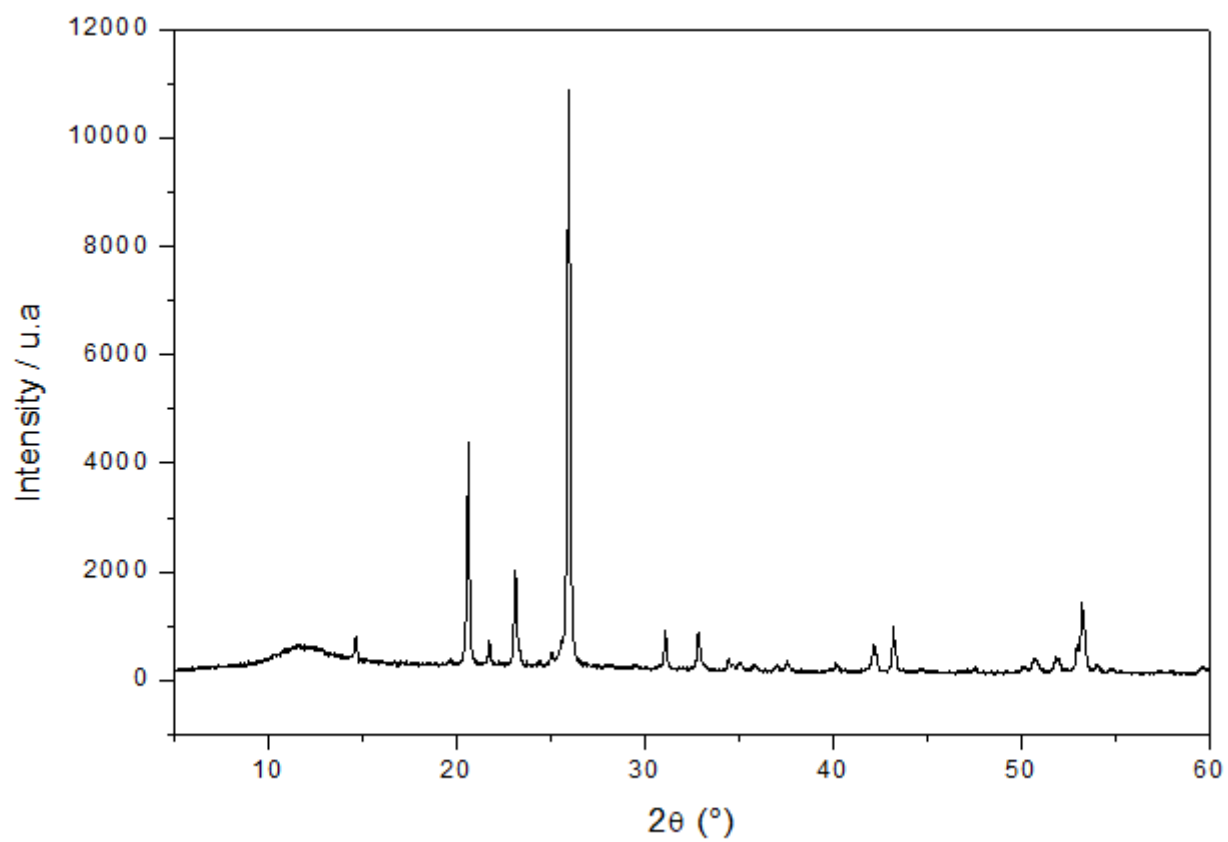


**Figure 4**

X-ray diffractogram of the thermolysis residue of HYP207·3H<sub>2</sub>O by TG / DTA

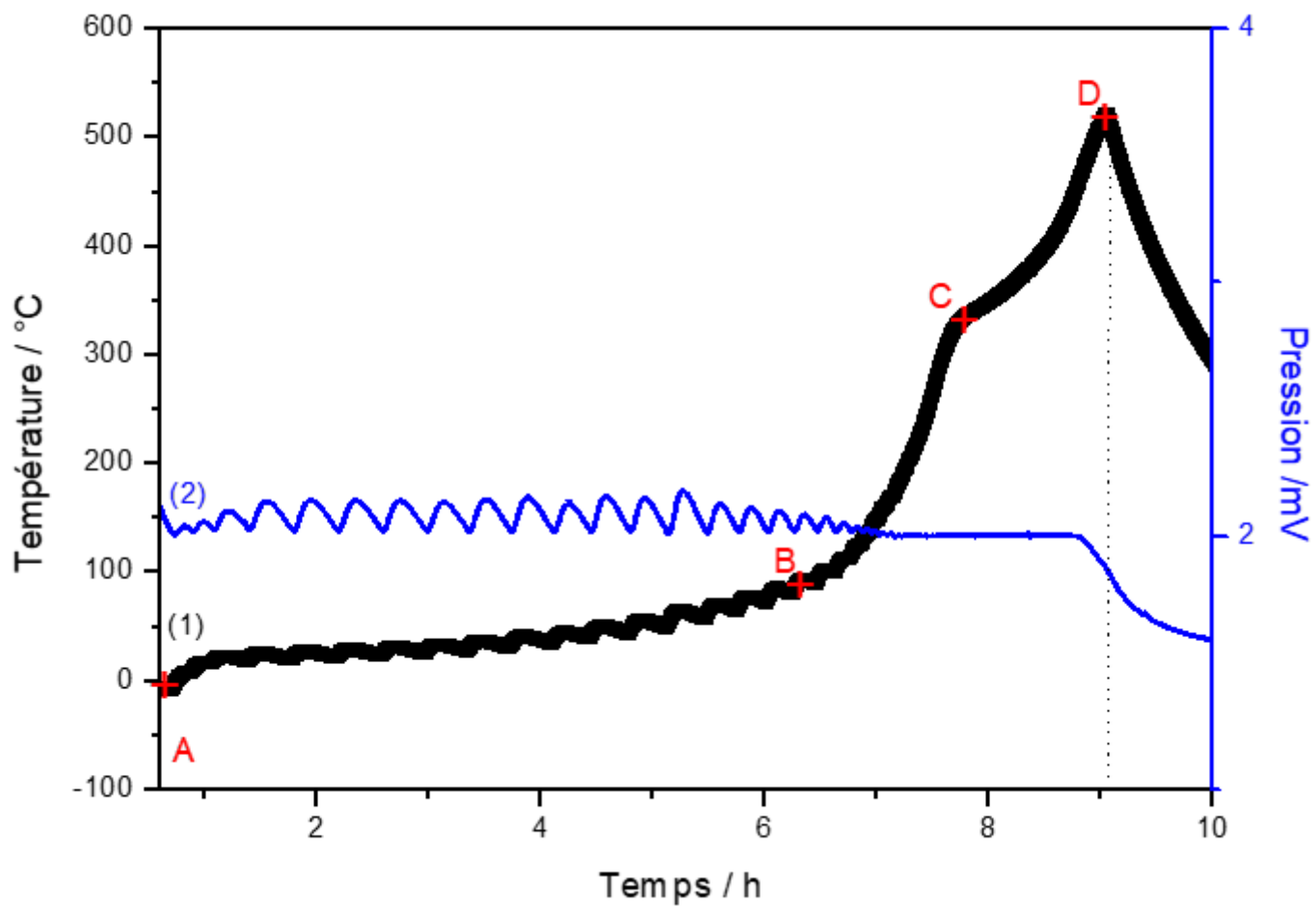
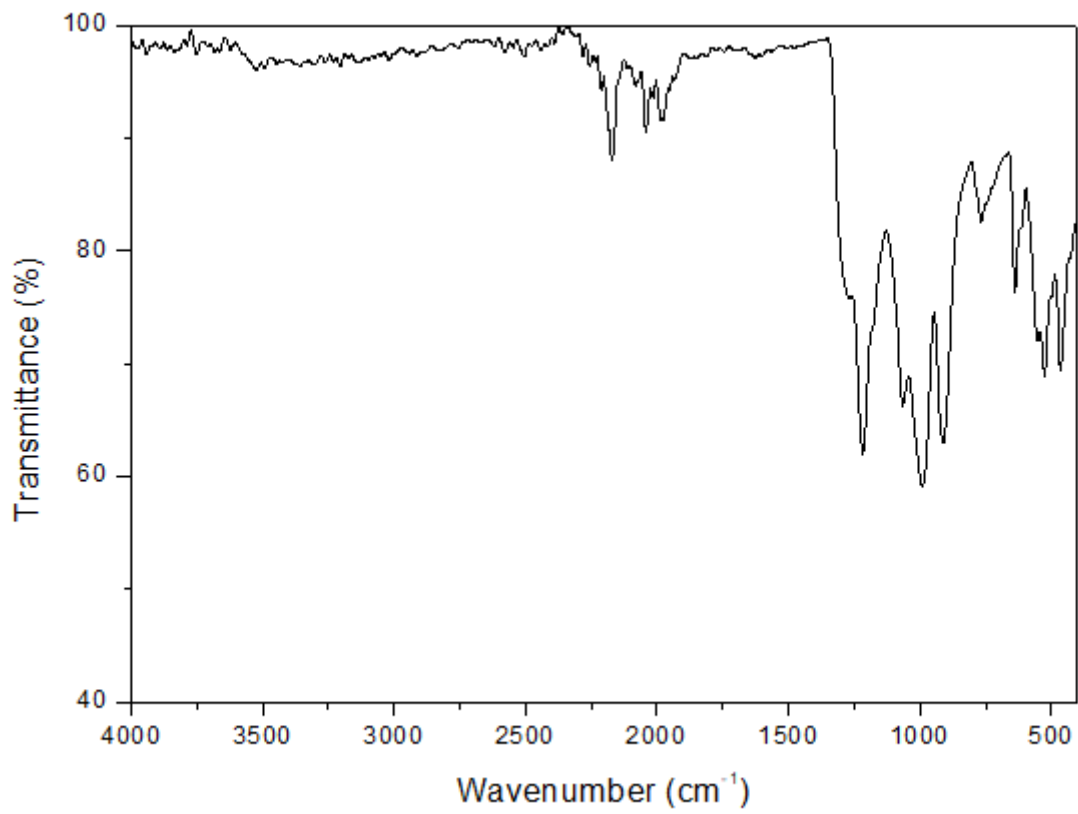


Figure 5

CRTA curves of HYP207·3H<sub>2</sub>O



**Figure 6**

IR Spectrum of the thermolysis residue of HYP2O7·3H2O by CRTA under 5hPa

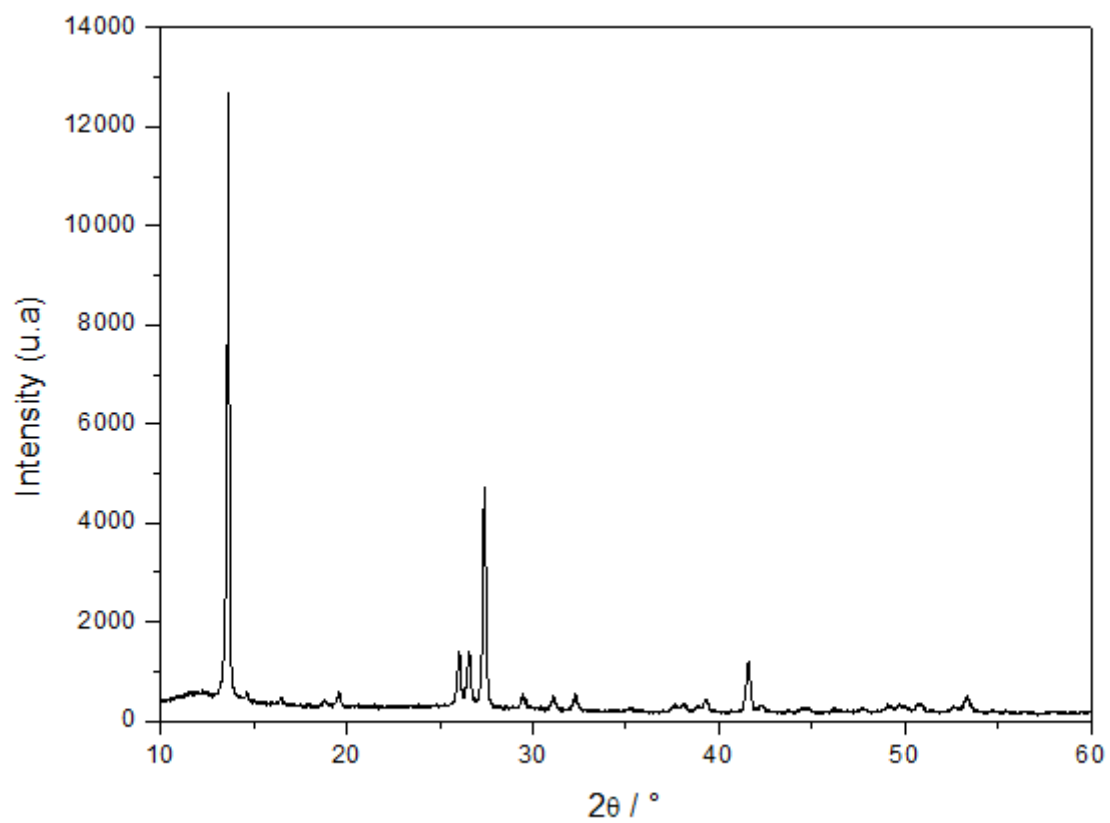


**Figure 7**

X-ray diffractogram of the thermolysis residue of HYP207·3H<sub>2</sub>O by CRTA under 5hPa

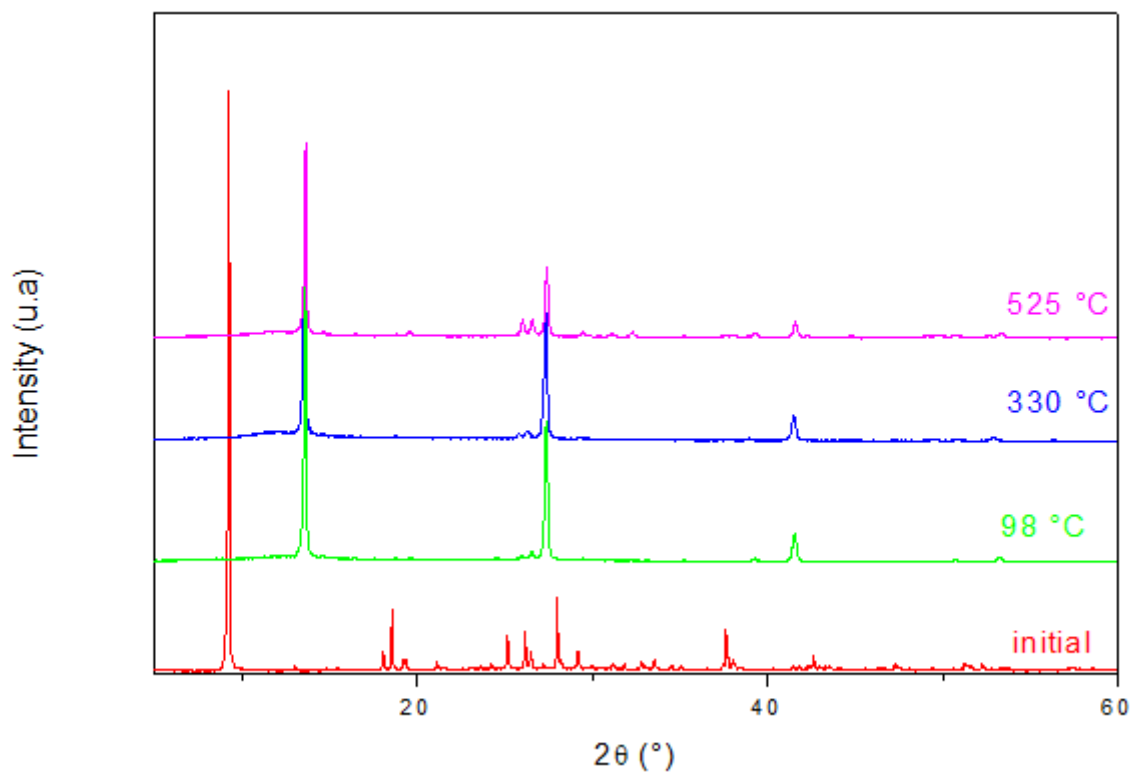


**Figure 8**

RX diffractograms of HYP207·3H<sub>2</sub>O (initial) and after treatment at different temperatures (° C) by CRTA under 5 hPa.

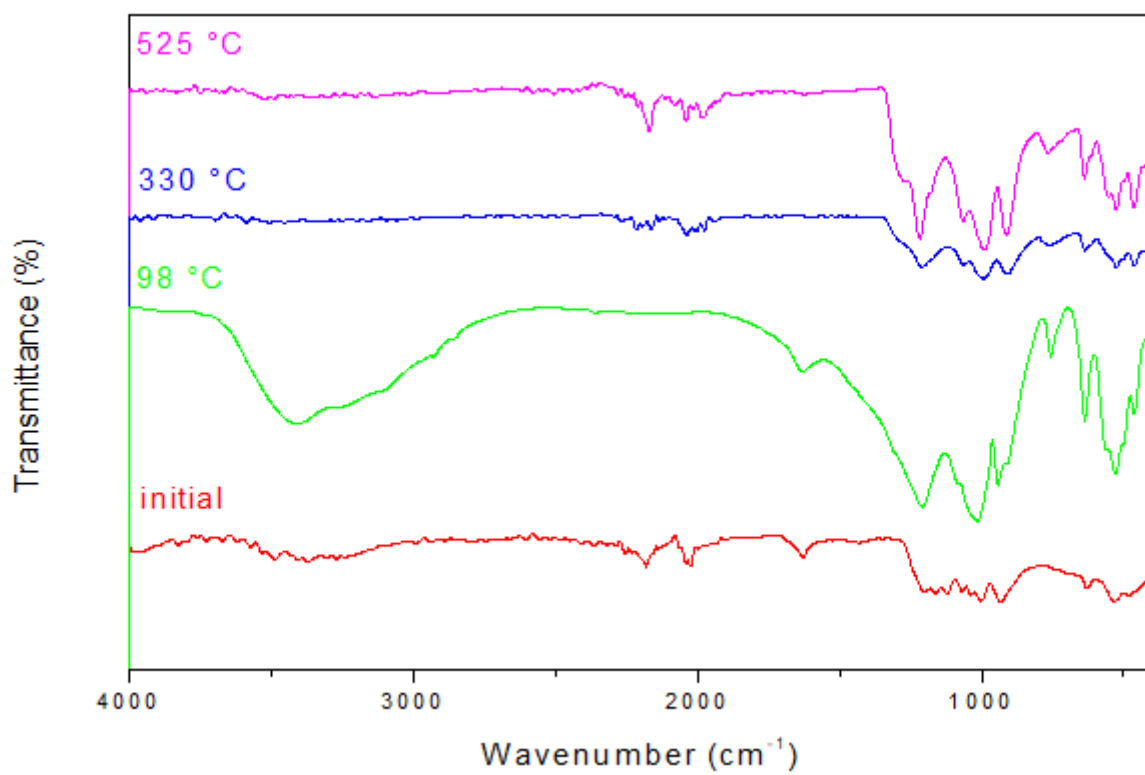
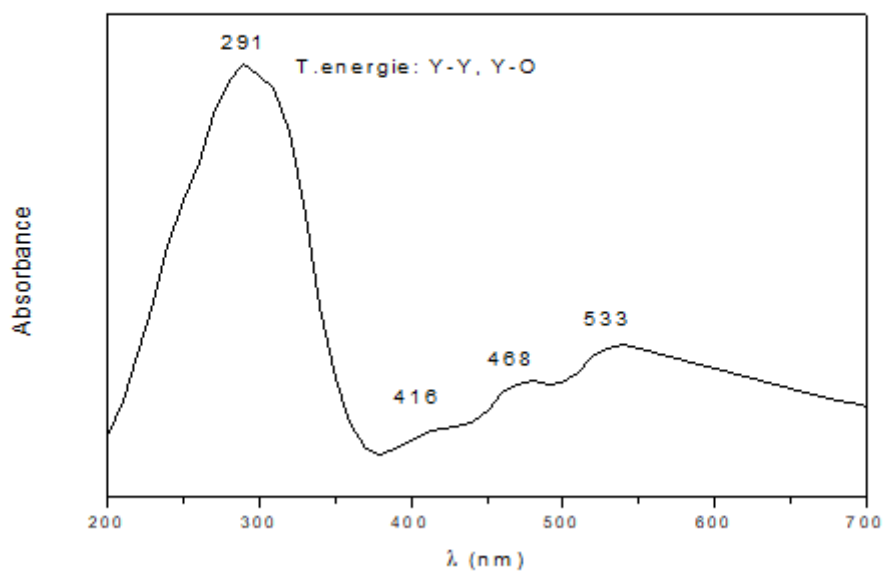


**Figure 9**

IR spectra of HYP207·3H<sub>2</sub>O (initial) and after treatment at different temperatures (° C) by CRTA under 5 hPa.

a



b

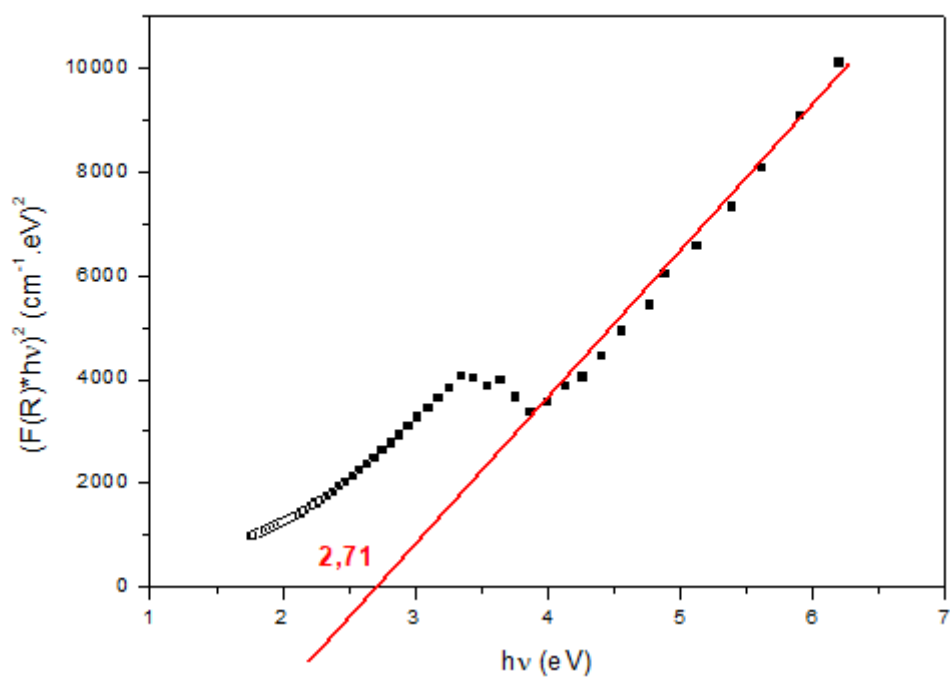
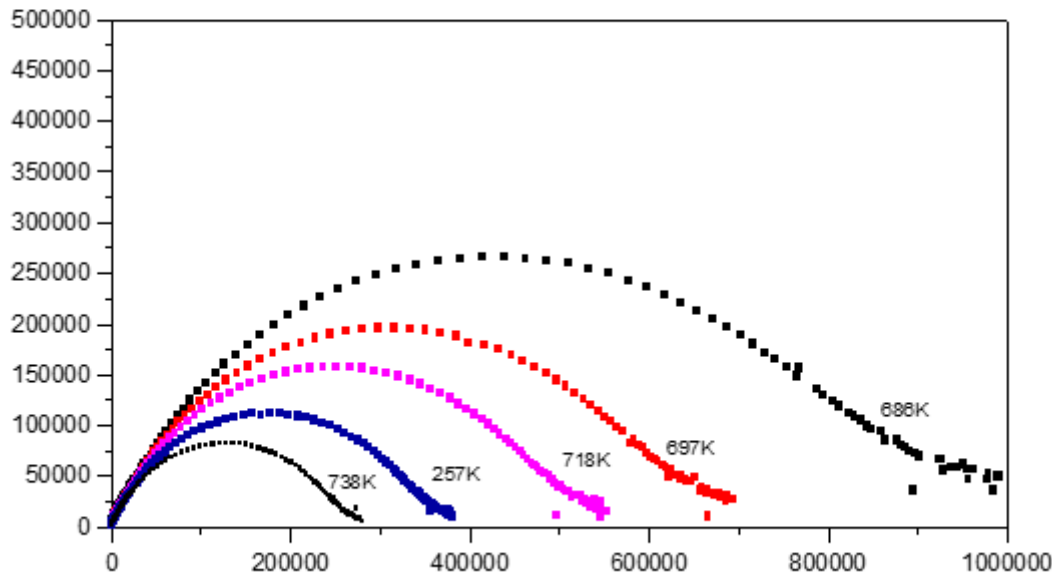
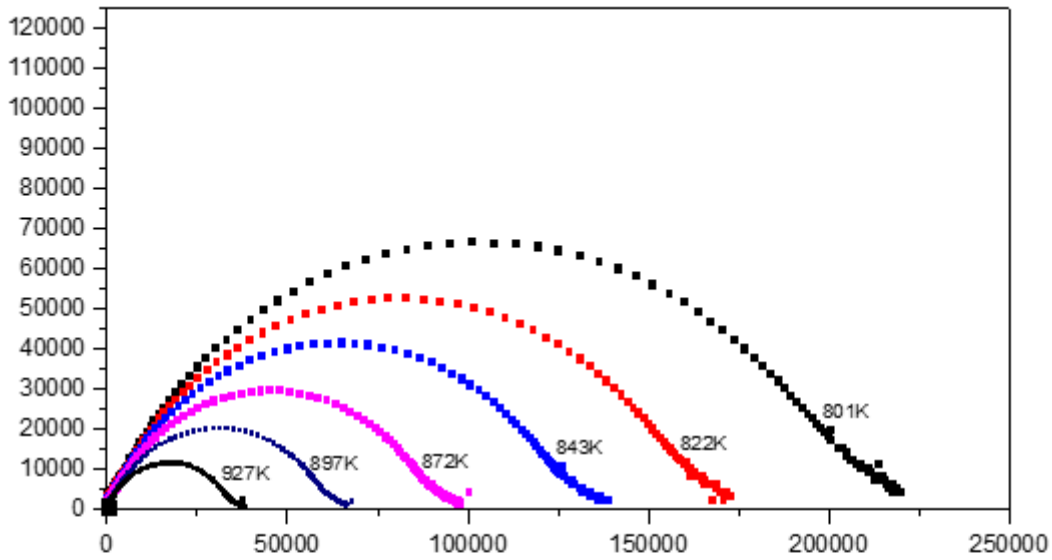


Figure 10

UV-Visible absorption spectrum(a) and UV diffuse reflectance spectrum (b) of the studied material



**Figure 11**

Nyquist plots of HYP207.

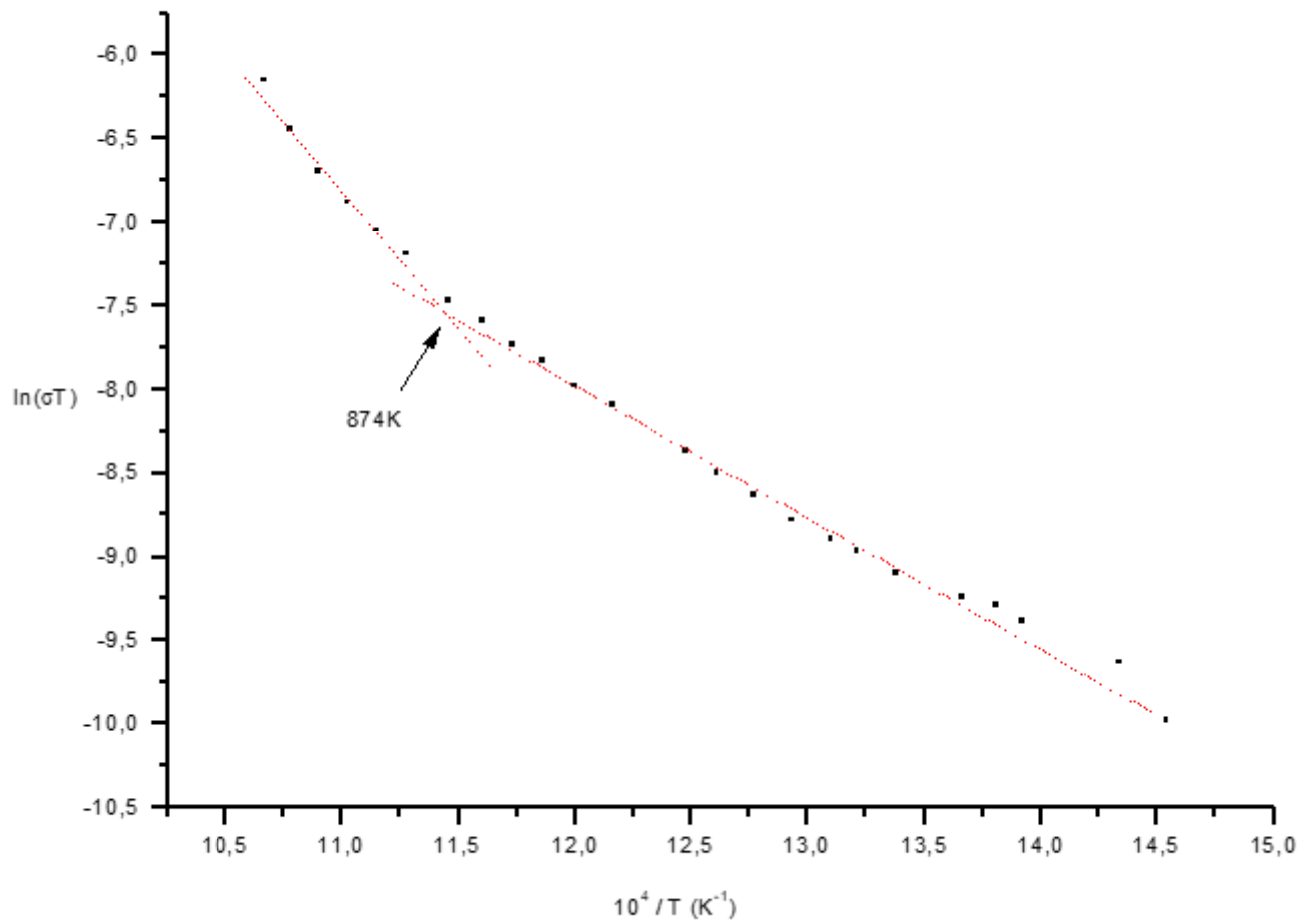


**Figure 12**

Arrhenius diagram of HYP207